HHS Public Access

Author manuscript

*Int J Radiat Oncol Biol Phys*. Author manuscript; available in PMC 2023 January 23.

Published in final edited form as:

*Int J Radiat Oncol Biol Phys*. 2022 November 15; 114(4): 725–737. doi:10.1016/j.ijrobp.2022.05.037.

# Tumor-Derived Extracellular Vesicles Predict Clinical Outcomes in Oligometastatic Prostate Cancer and Suppress Antitumor Immunity

**Fabrice Lucien, PhD**[*,†], **Yohan Kim, PhD**[*], **Jing Qian, PhD**[‡], **Jacob J. Orme, MD, PhD**[§], **Henan Zhang, MD**[†], **Ali Arafa, MD**[*], **Feven Abraha, MS**[‖], **Ishwor Thapa, MS**[¶], **Erik J. Tryggestad, PhD**[‡], **William S. Harmsen, PhD**[‖], **Jorgena Kosti, MD**[*], **Hesham Ali, PhD**[¶], **Val J. Lowe, MD**[#], **Geoff B. Johnson, MD**[#], **Eugene D. Kwon, MD**[*,†], **Haidong Dong, MD, PhD**[*,†], **Sean S. Park, MD, PhD**[‡]

[*]Department of Urology, Mayo Clinic, Rochester, Minnesota;

[†]Department of Immunology, Mayo Clinic, Rochester, Minnesota;

[‡]Department of Radiation Oncology, Mayo Clinic, Rochester, Minnesota;

[§]Department of Medical Oncology, Mayo Clinic, Rochester, Minnesota;

[‖]Departments of Biostatistics and Health Sciences Research, Mayo Clinic, Rochester, Minnesota;

[¶]Bioinformatics Core Facility, University of Nebraska Omaha, Omaha, Nebraska;

[#]Department of Radiology, Mayo Clinic, Rochester, Minnesota

## Abstract

**Purpose:** SABR has demonstrated clinical benefit in oligometastatic prostate cancer. However, the risk of developing new distant metastatic lesions remains high, and only a minority of patients experience durable progression-free response. Therefore, there is a critical need to identify which patients will benefit from SABR alone versus combination SABR and systemic agents. Herein we provide, to our knowledge, the first proof-of-concept of circulating prostate cancer-specific extracellular vesicles (PCEVs) as a noninvasive predictor of outcomes in oligometastatic castration-resistant prostate cancer (omCRPC) treated with SABR.

**Methods and Materials:** We analyzed the levels and kinetics of PCEVs in the peripheral blood of 79 patients with omCRPC at baseline and days 1, 7, and 14 after SABR using nanoscale flow cytometry and compared with baseline values from cohorts with localized and widely metastatic prostate cancer. The association of omCRPC PCEV levels with oncological outcomes was determined with Cox regression models.



Corresponding author: Fabrice Lucien-Matteoni, PhD; lucien-matteoni.fabrice@mayo.edu.

Disclosures: F.L. was the recipient of a postdoctoral fellowship from the Fonds de Recherche du Quebec-Sante. All other authors have no disclosures to declare.

Supplementary material associated with this article can be found, in the online version, at doi:10.1016/j.ijrobp.2022.05.037.

**Results:** Levels of PCEVs were highest in mCRPC followed by omCRPC and were lowest in localized prostate cancer. High PCEV levels at baseline predicted a shorter median time to distant recurrence (3.5 vs 6.6 months; $P = .0087$). After SABR, PCEV levels peaked on day 7, and median overall survival was significantly longer in patients with elevated PCEV levels (32.7 vs 27.6 months; $P = .003$). This suggests that pretreatment PCEV levels reflect tumor burden, whereas early changes in PCEV levels after treatment predict response to SABR. In contrast, radiomic features of $^{11}$C-choline positron emission tomography and computed tomography before and after SABR were not predictive of clinical outcomes. Interestingly, PCEV levels and peripheral tumor-reactive CD8 T cells ($T_{TR}$; $CD8^+$ $CD11a^{high}$) were correlated.

**Conclusions:** This original study demonstrates that circulating PCEVs can serve as prognostic and predictive markers to SABR to identify patients with "true" omCRPC. In addition, it provides novel insights into the global crosstalk, mediated by PCEVs, between tumors and immune cells that leads to systemic suppression of immunity against CRPC. This work lays the foundation for future studies to investigate the underpinnings of metastatic progression and provide new therapeutic targets (eg, PCEVs) to improve SABR efficacy and clinical outcomes in treatment-resistant CRPC.

## Introduction

Patients with metastatic castration-resistant prostate cancer (mCRPC) who progress after chemotherapy and next-generation antiandrogen therapy experience a meager median survival of 13.6 months.[1] A subset of these patients with oligometastatic disease, usually defined as ≤5 lesions, are ideal candidates for potentially curative SABR.[2] Indeed, 2 recent phase 2 randomized trials in oligometastatic castration-sensitive prostate cancer (CSPC) showed that SABR prolongs progression-free survival with minimal toxicity.[3,4] However, distant failure after SABR remains the primary manifestation of disease progression. In a separate phase 2 trial in oligometastatic CRPC (≤3 lesions) identified with $^{11}$C choline positron emission tomography (PET) and computed tomography (CT), SABR was very effective for local control (75% at 2 years).[5] Unfortunately, the median time to distant recurrence was 5.1 months, and 19% of patients experienced distant recurrence within 3 months. This suggests that advanced PET imaging may not be sufficiently sensitive. Thus, a combination of PET imaging and minimally invasive biomarkers could improve the selection of truly oligometastatic CRPC.[6]

Part of the benefit of SABR stems from the induction of a systemic antitumor immune response.[5,7–9] Peripheral expansion of clonotypic and tumor-reactive CD8 T cells is a prerequisite for local antitumor response and abscopal effect.[5,10,11] Thus, there is a critical need to understand the systemic suppression of anti-prostate cancer immunity, particularly in patients treated with SABR. This will provide a rationale to develop effective combination therapies as currently tested in melanoma, renal cell carcinoma, and lung cancer.[12,13]

Extracellular vesicles (EVs) are emerging as promising liquid biomarkers for cancer diagnosis and prognosis and prediction of treatment response.[14] EVs are nanosized vesicles released by all cell types, including tumor cells. They contain surface molecules and cargo from donor cells and travel in body fluids including blood and urine. The clinical utility

of EVs in the management of prostate cancer has been an active area of investigation.[15,16] Markers that reliably identify prostate cancer-derived EVs (PCEVs) are needed, and prostate cancer-specific markers and STEAP1 are strong potential candidates.[17] Importantly, clinical data investigating a role for EVs in patient selection and response monitoring have not been documented. Given the observation that clinical interventions affect EV subpopulations in a variable manner, it is essential to identify and validate these markers as they relate to tumor burden, treatment response, and antitumor immunity.[18]

Herein, we defined and examined baseline and post-SABR PCEV levels in a cohort of patients with omCRPC treated with SABR. We evaluated their performance as markers of disease burden and predictors of risk of distant failure in response to SABR. Finally, we investigated the association of PCEVs with peripheral CD8 T cells to gain novel biological insights on the crosstalk between tumor and immune cells in response to radiation therapy.

## Materials and Methods

### Patient cohort

A total of 89 patients with oligometastatic castration-refractory prostate cancer were identified with $^{11}$C-choline PET/CT and treated with SABR at Mayo Clinic between August 2016 and December 2019. Patients with ≤3 extracranial lesions, testosterone levels <50 ng/dL on androgen deprivation therapy, an Eastern Cooperative Oncology Group performance status score of 0 to 2, and >6 months of life expectancy were eligible. According to Guckenberger and colleagues' classification of oligometastatic disease,[19] 40 patients (50.6%) experienced repeat oligoprogression, whereas 35 patients (44.3%) experienced metachronous oligoprogression and 4 patients (5.1%) experienced induced oligoprogression. Study approval was granted by the Mayo Clinic Institutional Review Board (IRB #16–000785). The study was conducted in accordance with the Declaration of Helsinki, and written informed consent was obtained from all participants before enrollment. Whole blood was collected at baseline and at 3 time points after SABR (days 1, 7, and 14). In all, 79 of 89 patients provided blood at baseline. Of those 79 patients, 66 patients gave samples at baseline and day 7 after SABR. A total of 53 patients provided blood for all time points. A separate cohort of 40 patients with widely metastatic CRPC (mCRPC) (ie, patients with >3 metastatic lesions) detected by conventional CT and/or bone scan and with a prostate-specific antigen (PSA) level greater than 2.0 ng/mL was used to compare PCEV levels between patients with omCRPC and mCRPC (IRB #21–004451). Blood was also collected in a cohort of 22 men undergoing radical prostatectomy (RP) for localized prostate cancer. All men presented with undetectable PSA levels at the time of blood collection (within 4 months after RP) (IRB #19–011292).

### Labeling of prostate cancer-derived extracellular vesicles (PCEVs)

The PCEVs were labeled using the following monoclonal antibodies: Alexa Fluor 647 conjugated PSMA (3E7 clone; Creative Biolabs) and Alexa Fluor 488 conjugated STEAP1 (SMC1 clone, Mayo Clinic Antibody Hybridoma Core) antibodies. The PSMA and STEAP1 antibodies were conjugated using protein labeling kits (A10235 and A20173, Thermo Fisher Scientific). The degree of antibody labeling (DOL) was measured using a Nanodrop

One$^{C}$ spectrophotometer (Thermo Fisher Scientific). The degree of antibody labeling for PSMA and STEAP1 was 3.2 and 3.6, respectively. Antibody sensitivity and specificity were validated in vitro by using the human prostate cancer LNCaP (PSMA$^{+}$ STEAP1$^{+}$), PC3-flu (PSMA$^{-}$ STEAP1$^{-}$), and PC3-PIP (PSMA$^{+}$ STEAP1$^{-}$) cell lines. PC3-flu and PC3-PIP cell lines were kindly provided by Dr Xinning Wang (Case Comprehensive Cancer Center, Cleveland, Ohio). PSMA and STEAP1 protein expression in cell lines was validated by Western blot (Fig. E1A, E1B). Cell lines were cultured in serum-free media for 24 hours, and the conditioned medium was collected and concentrated using ultrafiltration (Amicon Ultra-15 100 kDa, Millipore). PSMA$^{+}$ and STEAP1$^{+}$ EVs were analyzed by nanoscale flow cytometry (Fig. E1C, E1D). Optimal antibody concentrations were determined by titration using 3 plasma samples with detectable levels of PSMA$^{+}$ and STEAP1$^{+}$ EVs. To confirm the specificity of PSMA and STEAP1 antibodies, plasma samples were treated with detergent (0.1% Sodium Dodecyl Sul-fate) for 30 minutes on ice followed by antibody staining (Fig. E2). Loss of >90% of fluorescent events in the presence of detergent would confirm that PSMA and STEAP1 antibodies recognized intact EVs and did not form false-positive aggregates.

## Nanoscale fiow cytometry

Platelet-poor plasma samples were thawed at 37°C for 1 minute and centrifuged at 13,000 × g for 5 minutes at room temperature. Platelet-poor plasma was diluted in sterile Phosphate-buffered saline filtered 0.22 $\mu$m and incubated for 30 minutes at room temperature with fluorescently labeled PSMA and STEAP1 antibodies. Labeled samples were further diluted in sterile Phosphate-buffered saline before analysis by nanoscale flow cytometry. Each plasma sample was analyzed on an Apogee A60-Micro Plus (Apogee FlowSystems Inc, Northwood, United Kingdom) equipped with 3 excitation lasers (405, 488, and 638 nm) and 9 detectors. Side scatter (Large Angle Light Scatter) was used as a trigger at a 405-nm laser wavelength. Particle detection by A60-Micro Plus was calibrated with Rosetta calibration beads according to the manufacturer's instructions (Exometry Inc). Before each run, a blank sample with Dulbecco's Phosphate-buffered Saline was analyzed to ensure a count rate <100 events per second. For each sample run, the event rate was kept below 7700 events per second to avoid a swarm effect.[20] Each sample was run in 3 technical replicates for 1 minute, and coefficient variation was kept below 15%. Data analysis was performed using FlowJo, version 10.6.1 (Tree Star, Palo Alto, California). The number of detected events, sample dilution, flow rate, and acquisition time were used to determine particle concentration (EVs per milliliter). For a detailed description of flow cytometer specifications and preanalytical and analytical procedures, please refer to the MIFlowCyt-EV report in Appendix E1 (Supplementary Materials).

## PET/CT imaging data analysis

$^{11}$C-choline PET and CT were performed for all patients. Quantitative image features extracted from PET/CT images included the region of interest (ROI) volume, ROIMaxHU, ROIMeanHU, ROIMaxSUV, ROIMeanSUV, TotalVolume, and TotalGlycolysis (HU = Hounsfield Unit; SUV = Standard Uptake Value). These 7 features were chosen because they are likely to correlate with the tumor or metastasis burden and can be divided into 2

groups based on the ROI selected by the algorithm described later and the sum of the total treatment volume.

To select the ROI, baseline PET/CT scans were first registered rigidly to the planning CT for each treated site, and the clinical target volume (CTV) high volume (defined by the treating physician) was copied to PET/CT. For patients with multiple lesions treated, the maximum SUV of each lesion was compared, and the volume with the highest SUV was selected as the ROI. The volume of the ROI is reported as ROIVolume.

To normalize the interpatient variation of the PET SUV and CT HU, a slice of descending aorta (DA) was contoured by a nuclear medicine physician, and the mean SUV from PET (DAM-eanSUV) and its mean HU from CT (DAM-eanHU) were calculated. The ROI-based values (ROI-MaxHU, ROIMeanHU, ROIMaxSUV, and ROIMeanSUV) were normalized by dividing by the DAMeanHU and the DAMeanSUV, respectively.

TotalVolume and TotalGlycolysis were not based on a selected ROI but on the sum of all treated sites. TotalVolume is the sum of all volumes treated. TotalGlycolysis is the sum of the product of the mean SUV and the treated volume of each site.

### Threshold optimization

To identify optimal cut-point values for each variable, we used a bioinformatic method adapted from the X-tile method.[21] The optimized cut value of each quantitative feature was obtained by minimizing the *P* value of a log-rank test with the exhaustive search method. To remove the effects of outliers, the 80th and 20th percentiles were used as the maximum and minimum of the search range for each feature, which was again divided into 50 intervals (steps) linearly. Starting from the minimum, the cut value was incremented step by step. At each step, the data set was divided by the cut value into 2 groups, and the log test *P* value for the 2 groups was calculated if the ratio of the group sizes was between 0.33 and 3.0. This constraint prevented extreme splitting of the data set. The cut value with the minimum *P* value was taken as the optimized cut value of the feature. To check the stability of the cut, the optimized cut value was shifted by 3% (either in the positive or negative direction), and the *P* value was calculated with the shifted cut value. The Python Lifelines module was used for log-rank and Kaplan-Meier tests.

### Immunophenotyping of peripheral CD8 T cells

Peripheral Blood Mononuclear Cells values were isolated, and subpopulations were identified with the following antibody panel: CD8-PE-Cy7 (BD Pharmingen, clone RPA-T8, catalog 304006), CD11a-APC (BioLegend, clone HI111, catalog 301212), PD-1 FITC (BioLegend, clone EH12.2H7, catalog 32990), Bim-PE (Cell Signaling Technology, clone CD34C5, catalog 12186S), Granzyme B-PerCP (Novus Biologicals, clone CLB0GB11, catalog NBP1–50071PCP), and CX3CR1-APC/Cy7 (BioLegend, clone 2A9–1, catalog 341616). Flow cytometry was performed on a CytoFLEX LX (Beckman Coulter, Atlanta, Georgia). Data were analyzed with FlowJo, version 10.6.1.

### Statistical analysis

Progression of PSA, distant failure, and overall survival were used as clinical endpoints to determine the association of PCEV levels with oncological outcomes. Kaplan-Meier estimates were used to estimate survival curves. For each Kaplan-Meier plot, *P* values were derived from the log-rank test for differences between groups. The hazard ratio (HR) of each biomarker was calculated with a univariate Cox proportional hazards model with different survival targets (PSA progression, distant recurrence, and overall survival). To minimize the effect of outliers, the biomarker values were capped by 2 times the 95th percentile value and standardized with the StandardScaler algorithm in the Python scikit-learn package. The association of PCEV levels with clinical features was determined using 2-sided Mann-Whitney *U* tests. Linear regression analysis of PCEV levels with imaging features or levels of peripheral CD8 T cells was used to determine Spearman *r* values and associated *P* values. For correlative studies, PCEV levels were treated as continuous variables. For association with clinical features and oncological outcomes, PCEV levels were converted to categorical variables and used to classify patients as high and low. Prism, version 9.0.1 (GraphPad Software), Python SciPy, and Python scikit-learn packages were used for all statistical analyses.

## Results

### Association of PCEV levels with tumor burden in oligometastatic and metastatic prostate cancer

To enumerate PCEVs directly from patient plasma, we used nanoscale flow cytometry and antibodies against the 2 well-known prostate markers PSMA and STEAP1 (Fig. 1A). We compared the levels of $PSMA^+$ EVs and $STEAP1^+$ EVs in the blood of patients with localized prostate cancer after radical prostatectomy (post-RP), patients with omCRPC, and patients with mCRPC (Fig. 1B–C). In the post-RP cohort, all men presented with an undetectable PSA level at the time of blood collection (≤4 months post-RP). The matched cohort of patients with mCRPC comprised heavily treated patients with widespread metastatic lesions identified by conventional CT and/or bone scan. This cohort had significantly higher levels of $PSMA^+$ EVs compared with the omCRPC and post-RP cohorts (median, 24,625 EVs/mL [95% confidence interval {CI}, 17,000–31,750 EVs/mL] vs 9467 EVs/mL [95% CI, 7067–11,600 EVs/mL] vs 1467 EVs/mL [95% CI, 666.7–2000 EVs/mL], respectively). Higher levels of $STEAP1^+$ EVs were also observed in patients with mCRPC, with a median level of 105,350 EVs/mL (95% CI, 78,500–164,000 EVs/mL) compared with 19,067 EVs/mL (95% CI, 15,467–20,800 EVs/mL) for patients with omCRPC and 3333 EVs/mL (95% CI, 2400–5067 EVs/mL) for post-RP patients. Of 69 patients with omCRPC, 24 (30.4%) had $STEAP1^+$ EV concentrations in the range observed in patients with mCRPC.

### Association of baseline PCEV levels with PSA and $^{11}$C-choline PET/CT imaging in omCRPC

We further investigated the association of PCEV levels from the blood of patients with omCRPC with a tumor burden assessed by serum PSA levels and 11C-choline PET/CT imaging characteristics. Baseline patient, tumor, and SABR characteristics of patients in this study are summarized in Table E1. $PSMA^+$ and $STEAP1^+$ PCEVs were detectable

in all patients, and 74 of 79 patients (93.7%) had higher circulating STEAP1$^+$ EVs than PSMA$^+$ EVs at baseline (Fig. 2A). Median levels of STEAP1$^+$ EVs and PSMA$^+$ EVs were 19,067 (range, 6800–3,468,933) and 9467 (range, 6800–3,468,933) per microliter of plasma, respectively (Table E1). A correlation analysis showed a significant positive correlation between baseline PSMA$^+$ and STEAP1$^+$ EVs (Spearman $r$, 0.599; 95% CI, 0.430–0.727; $P = 5.54 \times 10^{-9}$). Patients were subgrouped based on low and high PCEV levels. At baseline, the cutoffs were 11,100 and 57,698 EVs/mL for PSMA$^+$ EVs and STEAP1$^+$ EVs, respectively. Serum PSA levels at baseline were significantly higher in patients with high levels of both PSMA$^+$ EVs (2.4 vs 0.52 ng/mL; $P = .002$) and STEAP1$^+$ EVs (2.7 vs 0.62 ng/mL; $P = .008$) (Fig. 2B). Correlation analysis using continuous variables showed significant but moderate positive correlation between baseline levels of PSMA$^+$ EVs and PSA (Spearman $r$, 0.327; 95% CI, 0.108–0.516; $P = .003$). No significant correlation was observed between serum PSA levels and baseline concentrations of STEAP1$^+$ EVs (Spearman $r$, 0.210; 95% CI, −0.018 to 0.418; $P = .063$).

In the omCRPC cohort, 67.1% of patients had 1 extracranial metastatic lesion, 25.3% had 2 lesions, and 7.6% had 3 lesions detected by 11C-choline PET/CT imaging (Table E1). We analyzed the relationship between baseline PCEV levels and several PET/CT imaging parameters (Table E2). No significant association was observed between levels of STEAP1$^+$ EVs and tumor volume or characteristics within this cohort. Higher levels of PSMA$^+$ EVs were associated with increased ROI Max HU (CT) ($P = .03$), total volume ($P = .09$), and total glycolysis ($P = .07$). No correlation was found between PCEV levels and imaging features (Table E3). No association between PCEV levels and the number of metastatic lesions detected on $^{11}$C-choline PET/CT imaging was observed (Fig. 2C).

## Baseline PCEVs and risk of distant failure in omCRPC treated with SABR

Although SABR improves outcomes in oligometastatic prostate cancer, distant failure remains the major source of disease progression.[3,5] Some patients with limited metastatic burden (≤3–5 metastatic lesions) benefit significantly from SABR, but the identification of these patients remains challenging. To identify potential predictors of distant failure, we performed Cox univariate analysis with baseline clinical factors including PSA levels and PET imaging characteristics. No significant association was observed between clinical factors and risk for distant failure (Fig. 3A).

In contrast, a significant association was observed between PCEV levels at baseline and risk for distant recurrence. Both higher baseline PSMA$^+$ EVs (HR, 1.35; 95% CI, 1.03–1.76; $P = .03$) and STEAP1$^+$ EVs (HR, 1.43; 95% CI, 1.09–1.86; $P = .01$) predicted a higher risk of distant recurrence. Furthermore, high baseline PSMA$^+$ EVs and STEAP1$^+$ EVs were associated with a shorter time to distant recurrence (Fig. 3B). The median times to distant recurrence were 6.6 months and 3.5 months for patients with low and high levels of PSMA$^+$ EVs, respectively ($P = .009$). At 6 months, distant failure occurred in 19.5% of patients with low PSMA$^+$ EVs and in 70.4% of patients with high PSMA$^+$ EVs. Similarly, the median times to distant recurrence were 5.7 months and 4.2 months for patients with low and high STEAP1$^+$ EVs, respectively ($P = .022$). The risk of distant failure at 6 months after SABR was 66.6% among patients with high STEAP1$^+$ EVs, compared with 50%

among patients with low STEAP1$^+$ EVs. No association was observed between baseline PCEV levels and PSA progression or overall survival (Fig. E3). Our data posit PCEVs as a potential independent prognostic factor for risk of distant recurrence in omCRPC treated with SABR. The lack of prognostic value of PET imaging characteristics suggests that PET imaging may underestimate the true (micro)metastatic burden of omCRPC, and undetected metastases may continue to grow, causing distant failure. Patients with PET-identified omCRPC presenting high PCEV concentrations may have a higher tumor burden than anticipated with PET imaging, and they can be more at risk of distant recurrence.

## Kinetics of circulating PCEVs in patients with omCRPC treated with SABR

We sought to determine the short-term effects of SABR on PCEV release by measuring blood PCEV concentrations at 1, 7, and 14 days after SABR. Median levels of PSMA$^+$ EVs rapidly increased at day 1 after SABR by 1.6-fold (95% CI, 1.2- to 2.0-fold; $P = .004$), reaching a 2.1-fold (95% CI, 1.4-to 3.0-fold; $P < .0001$) increase at day 7 after SABR (Fig. 4A). At day 14 after SABR, median levels of PSMA$^+$ EVs regressed to baseline levels (1.2-fold increase; 95% CI, 0.9- to 1.8-fold increase; $P = .41$). For STEAP1$^+$ EVs, a similar trend was observed, with a median change compared with baseline of 1.1-fold (95% CI, 0.5- to 1.8-fold; $P = .18$), 2.1-fold (95% CI, 1.1- to 2.5-fold; $P = .0009$), and 1.5-fold (95% CI, 0.7- to 1.9-fold; $P = .17$) at days 1, 7, and 14 after SABR, respectively (Fig. 4B). Compared with baseline, levels of PSMA$^+$ EVs increased in 51 of 66 patients (77.2%) and decreased in 15 of 66 patients (22.8%) at day 7 after SABR (Fig. 4C). Levels of STEAP1$^+$ EVs increased in 44 of 66 patients (66.6%) and decreased in 22 of 66 patients (33.3%) (Fig. 4D). Changes in STEAP1$^+$ EV levels at day 7 after SABR were concordant with changes in PSMA$^+$ EVs for 43 of 66 patients (65.1%).

## Post-SABR PSMA$^+$ EVs and risk of distant recurrence and overall survival

Levels of post-SABR PSMA$^+$ EVs at day 7 were inversely associated with risk of distant recurrence (HR, 0.68; 95% CI, 0.48–0.97; $P = .03$) and overall survival (HR, 0.24; 95% CI, 0.1–0.8; $P = .02$) (Table E4). The median times to distant recurrence were 7.0 months and 3.3 months for high and low levels of PSMA$^+$ EVs, respectively ($P = 2.9 \times 10^{-4}$) (Fig. 5A). At 12 months' follow-up, distant failure occurred in 66.6% of patients with high levels of PSMA$^+$ EVs and 94.7% of patients with low levels of PSMA$^+$ EVs. Changes in levels of PSMA$^+$ EVs from baseline to day 7 were also predictors of distant recurrence (HR, 0.68; 95% CI, 0.49–0.93; $P = .02$) (Table E4). Post-SABR PSMA$^+$ EVs were associated with a higher risk of PSA progression (HR, 0.71; 95% CI, 0.5–1.0; $P = .06$). High post-SABR levels of PSMA$^+$ EVs at day 7 were also associated with a longer time to PSA progression (12.8 months vs 6.8 months; $P = .002$) and longer overall survival (32.6 months vs 27.6 months; $P = .003$) (Fig. 5B–C). For post-SABR STEAP1$^+$ EVs, no significant association was observed with outcomes. Finally, post-SABR PSA levels were associated with the risk of distant recurrence, but only PSA measurement at the earliest post-SABR time point (3 months) reached statistical significance ($P = .05$) (Fig. E4).

## Association of PCEV levels and immunologic changes

Preexisting antitumor immunity and expansion of tumor-reactive T cells are critical for response to SABR.[3,5] Patients with high levels of tumor-reactive T cells (CD11a$^{high}$ CD8$^+$)

responded better to SABR with prolonged PSA progression-free survival and time to distant recurrence.[5] Previous reports have demonstrated that tumor-derived EVs can carry immunosuppressive proteins and prevent immune-mediated tumor cell killing and response to immunotherapy.[22,23] In line with this, we performed a correlation analysis and evaluated the association between PCEV levels and peripheral CD8 T cells at baseline and after SABR (Fig. 6A). At baseline, we found that levels of both $PSMA^+$ and $STEAP1^+$ EVs correlated negatively with several subpopulations of tumor-reactive T cells (Table E5). No association was found between levels of parent tumor-reactive CD8 T cells ($CD11a^{high}$ $CD8^+$) and PCEVs (Fig. 6B). However, high baseline levels of $PSMA^+$ and $STEAP1^+$ EVs were associated with a lower percentage of tumor-reactive CD8 T cells positive for markers of effector function Bim, CX3CR1/GZMB, and PD-1 (Fig. 6C–E).[11,24] Conversely, elevated PCEV levels at day 7 correlated positively with tumor-reactive CD8 T cells at day 14 after SABR (Table E4 and Fig. 6F).

## Discussion

To our knowledge, this study is the first to analyze the kinetics and evaluate the clinical utility of tumor-derived EVs in patients with prostate cancer treated with radiation therapy. It is also the first study, to our knowledge, to evaluate an EV-based blood test as a complementary approach to $^{11}$C-choline PET/CT imaging for the diagnosis of oligometastatic prostate cancer. We analyzed the relationship between circulating EVs and peripheral CD8 T cells at baseline and post-SABR in the intent to provide novel insights in the crosstalk between tumors and immune cells.

SABR has shown clinical benefit in oligometastatic prostate cancer, but defining oligometastatic disease is challenging because it relies on imaging modalities with variable sensitivity and specificity.[3] There is a critical need to develop sensitive tools to assess tumor burden and identify patients with truly oligometastatic disease who can benefit the most from SABR.

Along with circulating tumor cells and circulating tumor DNA, EVs have recently emerged as potential markers of tumor burden and predictors of response to therapy.[22] To detect EVs released from prostate cancer, we used 2 prostate-specific surface markers, PSMA and STEAP1, previously found to be enriched in prostate cancer cells and EVs.[25,26] PSMA has received significant attention with the development of PSMA-directed radionuclide therapy and PET imaging.[27,28] Similarly, STEAP1 is currently under investigation as a molecular imaging marker and therapeutic target.[29,30] Interestingly, our study identified STEAP1 as a robust marker of tumor-derived EVs in CRPC. At the time of diagnosis, we observed a strong correlation between levels of $PSMA^+$ EVs and $STEAP1^+$ EVs in patients with CRPC. We also found that circulating $STEAP1^+$ EVs outnumbered $PSMA^+$ EVs in patients with omCRPC and mCRPC. Whereas antibody affinity can affect EV quantification, it may also indicate differential expression of PSMA and STEAP1 in CRPC. Low PSMA expression has been previously reported in treatment-refractory patients.[31] In response to androgen-deprivation therapy, CRPC tumors can progress toward a neuroendocrine phenotype and lose PSMA expression.[32] Notably, we detected PCEVs in all patients, including those with an undetectable PSA level at baseline. Intratumoral and intertumoral heterogeneity of

PSMA expression observed in advanced prostate cancer may have important consequences for patient selection using PSMA PET imaging and treatment with Lutetium-PSMA.[31] In a phase 1 study evaluating the safety profile of an antibody-drug conjugate targeting STEAP1, 99% of patients (133 of 134) showed positive STEAP1 expression, 73% with midhigh intensity.[30] Herein, we provide blood-based evidence that STEAP1 can be a promising alternative to PSMA for identification of aggressive prostate cancers, including those characterized by neuroendocrine features and low serum PSA levels. In line with this, a recent study in lung cancer found that STEAP1 is overexpressed in poorly differentiated neuroendocrine lung cancer (small cell lung carcinoma) compared with carcinoid tumors.[33] Further studies are warranted to determine differential expression of PSMA and STEAP1 in metastatic prostate cancer lesions identified by PET imaging.

To improve the selection of patients with oligometastatic prostate cancer, we determined the association of baseline PCEV levels and tumor burden assessed by 11C-choline PET imaging. Surprisingly, we did not find any correlation between PCEV levels and imaging features; however, baseline levels of $PSMA^+$ EVs and $STEAP1^+$ EVs were predictors of distant failure. Patients with high PCEV levels were at increased risk of distant metastatic progression. This suggests that $^{11}$C-choline PET imaging may underestimate disease burden and fail to identify treatable metastases. A PCEV-based blood test may refine the identification of truly oligometastatic prostate cancer and patients who will benefit most from SABR therapy. Given the emergence of PSMA PET imaging, comparative studies are needed to further evaluate the potential of PCEV levels as a marker of disease burden in patients with oligometastatic disease diagnosed with PSMA and/or choline PET imaging.

Longitudinal analysis after SABR revealed that blood PCEV levels increase rapidly after treatment and peak at day 7. Although irradiation has been shown to stimulate EV biogenesis with in vitro cell cultures,[34] the current study is, to our knowledge, the first clinical demonstration of SABR-induced EV release. $PSMA^+$ EVs at day 7 after SABR were a strong predictor of outcomes. In contrast to baseline levels, high levels of $PSMA^+$ EVs at day 7 were associated with a lower risk of disease progression and better survival. This suggests that an increase in blood $PSMA^+$ EV levels may indicate SABR-associated cancer cell death and antitumor immunity. Previous studies established that the expansion of peripheral tumor-reactive CD8 T cells after SABR is essential for local and systemic tumor control.[3,5] Herein, we found that elevation of PCEV was positively correlated with levels of tumor-reactive CD8 T cells. Interestingly, the highest correlation was observed with CD8 T cells expressing CX3CR1 chemokine receptor. CX3CR1 is expressed by effector CD8 T cells, and high levels of peripheral $CX3CR1^+$ CD8 T cells have been linked to better response to immune checkpoint blockade.[24,35] Although these findings suggest EV-mediated crosstalk between tumors and CD8 T cells, the nature of this association remains elusive. The peak of PCEV levels (day 7) preceded the increased frequency of tumor-reactive CD8 T cells (day 14), which suggests that PCEVs may play an active role in SABR-induced antitumor immunity. Similarly, in a prior study, patients with melanoma who responded to pembrolizumab immunotherapy had levels of $Ki67^+$ $PD1^+$ CD8 T cells that positively correlated with blood-derived exosomal PD-L1.[22] Tumor-derived EVs can carry immunomodulatory molecules such as PD-L1, CD73, miRNAs, and cytosolic DNA that either induce or inhibit antitumor immunity.[36–40] Prostate cancer is

characterized by an immunosuppressive tumor microenvironment, and EVs can contribute to tumor immune escape.[41–43] At baseline, we found an inverse correlation between PCEV and tumor-reactive CD8 T cells, which may indicate an inherently immunosuppressive environment driven by PCEVs. After SABR treatment, a subset of omCRPC patients have a durable response, with no signs of disease progression after 2 years. This suggests that in these best responders, SABR can alter the molecular composition of PCEVs toward an immunostimulatory phenotype resulting in abscopal response.[44,45] Conversely, limited control of distant metastases can be attributed to the release of immunosuppressive EVs that impair T-cell priming and tumor cell killing. PD-L1 and B7-H3 immune checkpoint molecules can be upregulated on the surface of EVs in response to radiation therapy.[46,47] Additional studies should focus on characterizing the molecular composition of PCEVs and determining the effect of SABR on expression of immuno-regulatory molecules. Furthermore, it is critical to decipher the molecular and cellular mechanisms involved in EV-mediated antitumor immunity in response to SABR using immunocompetent prostate cancer mouse models. This will pave the way for the design of biomarker-driven combination therapies, improving SABR efficacy and patient outcome.

We recognize several limitations to this study. First, our study may be underpowered. This, accompanied by its retrospective design, may introduce selection bias that confounds the study results. In this study, we used nanoscale flow cytometry as a means of establishing proof-of-concept of the clinical utility of measuring circulating tumor-derived EVs for patient stratification and prediction of response to SABR. Although this technology is not primarily designed for clinical use, it has already been implemented in several clinical studies including randomized controlled trials.[48–51] Nanoscale flow cytometry offers numerous advantages for developing EV-based blood tests. It allows for high throughput multiparametric detection of EVs of approximately 150 nm or greater. In addition, this technology has minimal requirements with respect to preanalytical steps necessary to obtain a robust EV-based assay. This is a particularly important consideration, because most studies evaluating the clinical benefit of EVs are limited by cost and time-consuming preanalytical procedures affecting data reproducibility and implementation in a clinic setting. Our blood test can be performed within 1 hour from the time of blood collection to data analysis using basic laboratory equipment, highlighting the potential for using such technology in the clinical setting with broad feasibility.

## Conclusions

This hypothesis-driven study sheds light on a new EV-based blood test that may improve identification of patients with oligometastatic castration-refractory prostate cancer who will benefit from SABR treatment. Additionally, it provides novel biological insights in the crosstalk between tumor cells and adaptive immune cells in response to SABR. Future endeavors will involve validation in larger patient cohorts and comprehensive profiling of the molecular cargo of prostate cancer-derived extracellular vesicles to refine risk prediction and identify potential therapeutic vulnerabilities to improve response to SABR.

## Supplementary Material

Refer to Web version on PubMed Central for supplementary material.

## Acknowledgments

This research was supported by National Cancer Institute R01 CA200551 (S.S.P., V.J.L., E.D.K., and H.D.), a departmental grant (F.L.), and generous benefactors (F.L.).

Mayo Clinic receives funding from ViewPoint, MedTrace, Clarity and AAA/Novartis for research conducted by GBJ. Mayo Clinic receives funding from ViewPoint, MedTrace, Pfizer, Blue Earth, AAA/Novartis and Curium for consulting by GBJ.

## Data sharing statement:

All data generated and analyzed during this study are included in this published article and its supplementary information files.

## References

1. de Wit R, de Bono J, Sternberg CN, et al. Cabazitaxel versus abiraterone or enzalutamide in metastatic prostate cancer. N Engl J Med 2019;381:2506–2518. [PubMed: 31566937]
2. Hellman S, Weichselbaum RR. Oligometastases. J Clin Oncol 1995;13:8–10. [PubMed: 7799047]
3. Phillips R, Shi WY, Deek M, et al. Outcomes of observation vs stereotactic ablative radiation for oligometastatic prostate cancer: The ORIOLE phase 2 randomized clinical trial [e-pub ahead of print]. JAMA Oncol. Available at: doi: 10.1001/jamaoncol.2020.0147. Accessed February 20, 2020.
4. Ost P, Reynders D, Decaestecker K, et al. Surveillance or metastasis-directed therapy for oligometastatic prostate cancer recurrence (STOMP): Five-year results of a randomized phase II trial. J Clin Oncol 2020;3:10.
5. Zhang H, Orme JJ, Abraha F, et al. Phase II evaluation of stereotactic ablative radiotherapy (SABR) and immunity in (11)C-choline-PET/CT-identified oligometastatic castration-resistant prostate cancer [e-pub ahead of print]. Clin Cancer Res. Available at: doi: 10.1158/1078-0432.CCR-21-2510. Accessed September 30, 2021.
6. Lennon AM, Buchanan AH, Kinde I, et al. Feasibility of blood testing combined with PET-CT to screen for cancer and guide intervention. Science 2020;369:eabb9601. [PubMed: 32345712]
7. Postow MA, Callahan MK, Barker CA, et al. Immunologic correlates of the abscopal effect in a patient with melanoma. N Engl J Med 2012;366:925–931. [PubMed: 22397654]
8. Dewan MZ, Galloway AE, Kawashima N, et al. Fractionated but not single-dose radiotherapy induces an immune-mediated abscopal effect when combined with anti-CTLA-4 antibody. Clin Cancer Res 2009;15:5379–5388. [PubMed: 19706802]
9. Demaria S, Kawashima N, Yang AM, et al. Immune-mediated inhibition of metastases after treatment with local radiation and CTLA-4 blockade in a mouse model of breast cancer. Clin Cancer Res 2005;11:728–734. [PubMed: 15701862]
10. Park SS, Dong H, Liu X, et al. PD-1 restrains radiotherapy-induced abscopal effect. Cancer Immunol Res 2015;3:610–619. [PubMed: 25701325]
11. Dronca RS, Liu X, Harrington SM, et al. T cell Bim levels reflect responses to anti-PD-1 cancer therapy. JCI Insight 2016;1:e86014. [PubMed: 27182556]
12. Watanabe T, Firat E, Scholber J, et al. Deep abscopal response to radiotherapy and anti-PD-1 in an oligometastatic melanoma patient with unfavorable pretreatment immune signature. Cancer Immunol Immunother 2020;69:1823–1832. [PubMed: 32350591]
13. Formenti SC, Rudqvist NP, Golden E, et al. Radiotherapy induces responses of lung cancer to CTLA-4 blockade. Nat Med 2018;24:1845–1851. [PubMed: 30397353]
14. Zhou E, Li Y, Wu F, et al. Circulating extracellular vesicles are effective biomarkers for predicting response to cancer therapy. EBioMedicine 2021;67:103365. [PubMed: 33971402]

15. Nanou A, Miller MC, Zeune LL, et al. Tumour-derived extracellular vesicles in blood of metastatic cancer patients associate with overall survival. Br J Cancer 2020;122:801–811. [PubMed: 31937922]
16. Del Re M, Biasco E, Crucitta S, et al. The detection of androgen receptor splice variant 7 in plasma-derived exosomal RNA strongly predicts resistance to hormonal therapy in metastatic prostate cancer patients. Eur Urol 2017;71:680–687. [PubMed: 27733296]
17. Lee JK, Bangayan NJ, Chai T, et al. Systemic surfaceome profiling identifies target antigens for immune-based therapy in subtypes of advanced prostate cancer. Proc Natl Acad Sci U S A 2018;115:E4473–E4482. [PubMed: 29686080]
18. Orme JJ, Enninga EAL, Lucien-Matteoni F, et al. Therapeutic plasma exchange clears circulating soluble PD-L1 and PD-L1-positive extracellular vesicles. J Immunother Cancer 2020;8:e001113. [PubMed: 32817395]
19. Guckenberger M, Lievens Y, Bouma AB, et al. Characterisation and classification of oligometastatic disease: A European Society for Radiotherapy and Oncology and European Organisation for Research and Treatment of Cancer consensus recommendation. Lancet Oncol 2020;21:e18–e28. [PubMed: 31908301]
20. van der Pol E, van Gemert MJ, Sturk A, Nieuwland R, van Leeuwen TG. Single vs. swarm detection of microparticles and exosomes by flow cytometry. J Thromb Haemost 2012;10:919–930. [PubMed: 22394434]
21. Camp RL, Dolled-Filhart M, Rimm DL. X-tile: A new bio-informatics tool for biomarker assessment and outcome-based cut-point optimization. Clin Cancer Res 2004;10:7252–7259. [PubMed: 15534099]
22. Chen G, Huang AC, Zhang W, et al. Exosomal PD-L1 contributes to immunosuppression and is associated with anti-PD-1 response. Nature 2018;560:382–386. [PubMed: 30089911]
23. Cox MJ, Lucien F, Sakemura R, et al. Leukemic extracellular vesicles induce chimeric antigen receptor T cell dysfunction in chronic lymphocytic leukemia. Mol Ther 2021;29:1529–1540. [PubMed: 33388419]
24. Yamauchi T, Hoki T, Oba T, et al. T-cell CX3CR1 expression as a dynamic blood-based biomarker of response to immune checkpoint inhibitors. Nat Commun 2021;12:1402. [PubMed: 33658501]
25. Pinto JT, Suffoletto BP, Berzin TM, et al. Prostate-specific membrane antigen: A novel folate hydrolase in human prostatic carcinoma cells. Clin Cancer Res 1996;2:1445–1451. [PubMed: 9816319]
26. Mariscal J, Vagner T, Kim M, et al. Comprehensive palmitoyl-proteomic analysis identifies distinct protein signatures for large and small cancer-derived extracellular vesicles. J Extracell Vesicles 2020;9: 1764192. [PubMed: 32944167]
27. Calais J, Ceci F, Eiber M, et al. $^{18}$F-fluciclovine PET-CT and $^{68}$Ga-PSMA-11 PET-CT in patients with early biochemical recurrence after prostatectomy: a prospective, single-centre, single-arm, comparative imaging trial. Lancet Oncol 2019;20:1286–1294. [PubMed: 31375469]
28. Sartor O, de Bono J, Chi KN, et al. Lutetium-177-PSMA-617 for metastatic castration-resistant prostate cancer. N Engl J Med 2021; 385:1091–1103. [PubMed: 34161051]
29. Carrasquillo JA, Fine BM, Pandit-Taskar N, et al. Imaging patients with metastatic castration-resistant prostate cancer using 89Zr-DFOMSTP2109A anti-STEAP1 antibody. J Nucl Med 2019;60:1517–1523. [PubMed: 31053681]
30. Danila DC, Szmulewitz RZ, Vaishampayan U, et al. Phase I study of DSTP3086S, an antibody-drug conjugate targeting six-transmembrane epithelial antigen of prostate 1, in metastatic castration-resistant prostate cancer. J Clin Oncol 2019;37:3518–3527. [PubMed: 31689155]
31. Thang SP, Violet J, Sandhu S, et al. Poor outcomes for patients with metastatic castration-resistant prostate cancer with low prostate-specific membrane antigen (PSMA) expression deemed ineligible for $^{177}$Lu-labelled PSMA radioligand therapy. Eur Urol Oncol 2019;2:670–676. [PubMed: 31412006]
32. Bakht MK, Derecichei I, Li Y, et al. Neuroendocrine differentiation of prostate cancer leads to PSMA suppression. Endocr Relat Cancer 2018;26:131–146. [PubMed: 30400059]
33. Prieto TG, Baldavira CM, Machado-Rugolo J, et al. Pulmonary neuroendocrine neoplasms overexpressing epithelial-mesenchymal transition mechanical barriers genes lack immune-

suppressive response and present an increased risk of metastasis. Front Oncol 2021;11 645623. [PubMed: 34527572]

34. Ramakrishnan V, Xu B, Akers J, et al. Radiation-induced extracellular vesicle (EV) release of miR-603 promotes IGF1-mediated stem cell state in glioblastomas. EBioMedicine 2020;55:102736. [PubMed: 32361246]
35. Vera Aguilera J, Paludo J, McWilliams RR, et al. Chemo-immunotherapy combination after PD-1 inhibitor failure improves clinical outcomes in metastatic melanoma patients. Melanoma Res 2020;30:364–375. [PubMed: 32404734]
36. Himes BT, Peterson TE, de Mooij T, et al. The role of extracellular vesicles and PD-L1 in glioblastoma-mediated immunosuppressive monocyte induction. Neuro Oncol 2020;22:967–978. [PubMed: 32080744]
37. Ricklefs FL, Alayo Q, Krenzlin H, et al. Immune evasion mediated by PD-L1 on glioblastoma-derived extracellular vesicles. Sci Adv 2018;4: eaar2766. [PubMed: 29532035]
38. Clayton A, Al-Taei S, Webber J, Mason MD, Tabi Z. Cancer exosomes express CD39 and CD73, which suppress T cells through adenosine production. J Immunol 2011;187:676–683. [PubMed: 21677139]
39. Wennerberg E, Spada S, Rudqvist NP, et al. CD73 blockade promotes dendritic cell infiltration of irradiated tumors and tumor rejection. Cancer Immunol Res 2020;8:465–478. [PubMed: 32047024]
40. Huber V, Vallacchi V, Fleming V, et al. Tumor-derived microRNAs induce myeloid suppressor cells and predict immunotherapy resistance in melanoma. J Clin Invest 2018;128:5505–5516. [PubMed: 30260323]
41. Salimu J, Webber J, Gurney M, Al-Taei S, Clayton A, Tabi Z. Dominant immunosuppression of dendritic cell function by prostate-cancer-derived exosomes. J Extracell Vesicles 2017;6:1368823. [PubMed: 28959385]
42. Lundholm M, Schrfioder M, Nagaeva O, et al. Prostate tumor-derived exosomes down-regulate NKG2D expression on natural killer cells and CD8+ T cells: Mechanism of immune evasion. PLoS One 2014;9: e108925. [PubMed: 25268476]
43. Poggio M, Hu T, Pai CC, et al. Suppression of exosomal PD-L1 induces systemic anti-tumor immunity and memory. Cell 2019;177 :414–427.e13. [PubMed: 30951669]
44. Diamond JM, Vanpouille-Box C, Spada S, et al. Exosomes shuttle TREX1-sensitive IFN-stimulatory dsDNA from irradiated cancer cells to DCs. Cancer Immunol Res 2018;6:910–920. [PubMed: 29907693]
45. Lin W, Xu Y, Chen X, et al. Radiation-induced small extracellular vesicles as “carriages” promote tumor antigen release and trigger anti-tumor immunity. Theranostics 2020;10:4871–4884. [PubMed: 32308755]
46. Vardaki I, Corn P, Gentile E, et al. Radium-223 treatment increases immune checkpoint expression in extracellular vesicles from the metastatic prostate cancer bone microenvironment. Clin Cancer Res 2021;27:3253–3264. [PubMed: 33753455]
47. Kim Y, Lavoie RR, Dong H, Park S, Abstract Lucien-Matteoni F. 675: Radiotherapy inhibits the antitumor immune response through release of immunosuppressive tumor-derived extracellular vesicles in prostate cancer. Cancer Research 2021;81:675–675.
48. Davidson TM, Foster N, Lucien F, et al. Rescuing cancer immunity by plasma exchange in metastatic melanoma (ReCIPE-M1): Protocol for a single-institution, open-label safety trial of plasma exchange to clear sPD-L1 for immunotherapy. BMJ Open 2022;12:e050112.
49. Chiva-Blanch G, Sala-Vila A, Crespo J, Ros E, Estruch R, Badimon L. The Mediterranean diet decreases prothrombotic microvesicle release in asymptomatic individuals at high cardiovascular risk. Clin Nutr 2020;39:3377–3384. [PubMed: 32147198]
50. Gąsecka A, Banaszkiewicz M, Nieuwland R, et al. Prostacyclin analogues inhibit platelet reactivity, extracellular vesicle release and thrombus formation in patients with pulmonary arterial hypertension. J Clin Med 2021;10:1024. [PubMed: 33801460]
51. Gasecka A, Nieuwland R, Budnik M, et al. Randomized controlled trial protocol to investigate the antiplatelet therapy effect on extracellular vesicles (AFFECT EV) in acute myocardial infarction. Platelets 2020;31:26–32. [PubMed: 30585111]

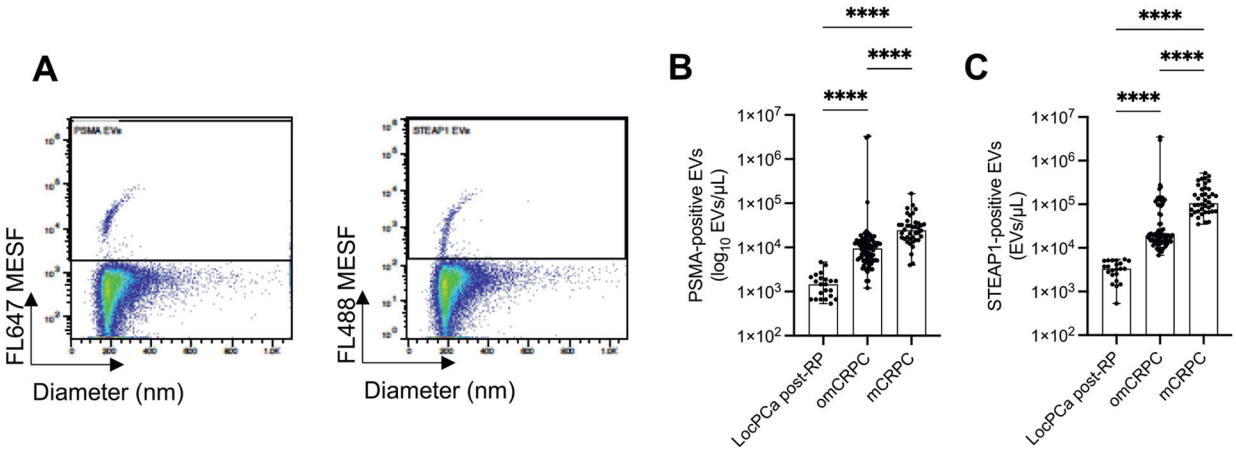


**Fig. 1.**

Association of prostate cancer–specific extracellular vesicle levels with tumor burden in oligometastatic and metastatic prostate cancer. (A) Representative scatterplots showing nanoscale flow cytometric detection of PSMA- and STEAP1-positive extracellular vesicles (EVs) from plasma of 1 patient with oligometastatic castration-resistant prostate cancer (omCRPC). (B, C) Comparisons are shown in levels of PSMA-positive (B) and STEAP1-positive EVs (C) in localized prostate cancer after radical prostatectomy (n = 22), omCRPC (n = 79), and metastatic castration-resistant prostate cancer (n = 40). ***$P < .001$ by Kruskal-Wallis test.

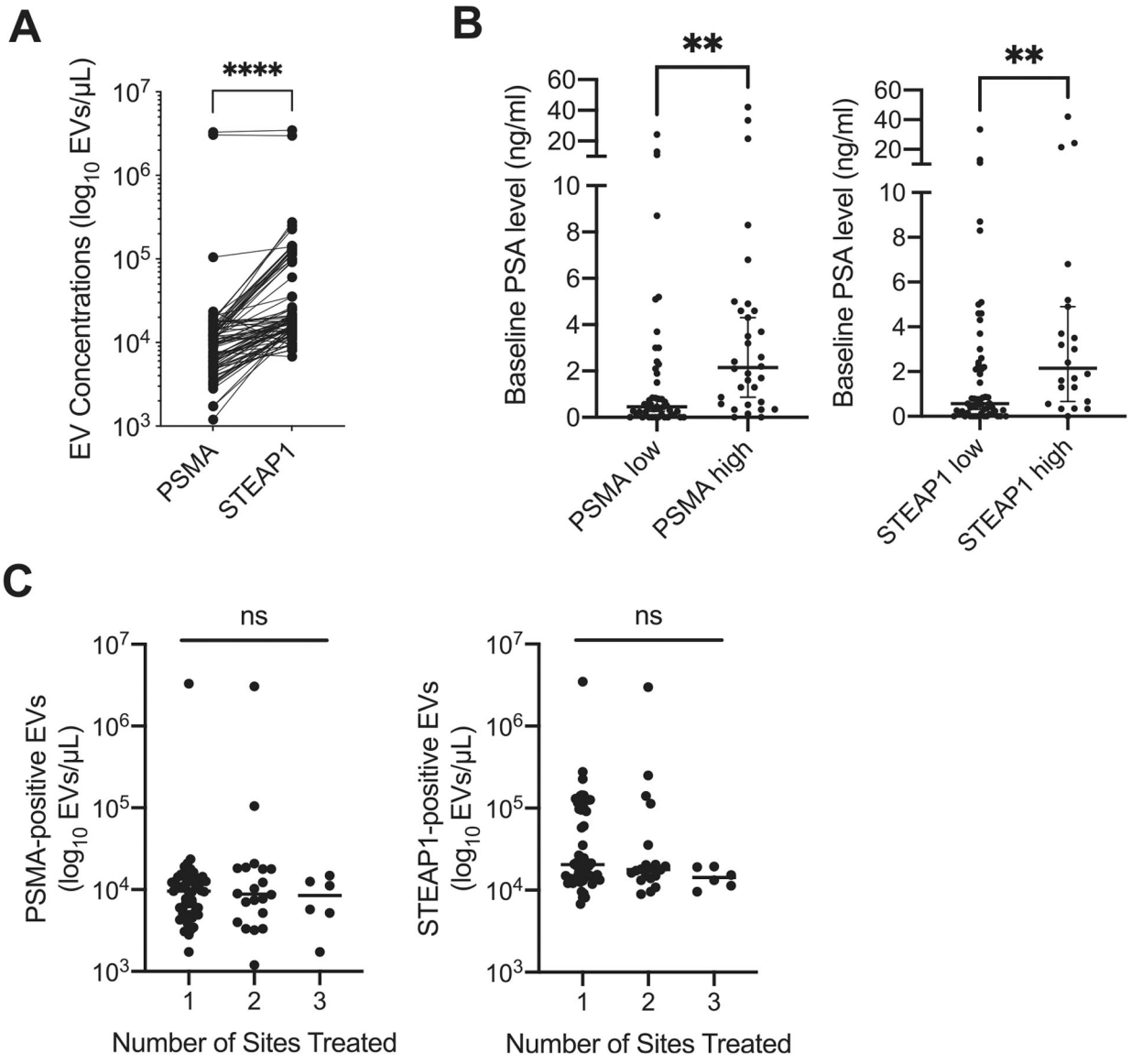


**Fig. 2.**

Baseline prostate cancerfispecific extracellular vesicle levels and association with prostate-specific antigen (PSA) and $^{11}$C-choline positron emission tomography (PET) imaging in patients with oligometastatic castration-resistant prostate cancer (omCRPC). (A) Baseline blood concentrations of PSMA- and STEAP1-positive extracellular vesicles (EVs) in patients with omCRPC (n = 79). Data are presented in a logarithmic scale. ***$P < .000$ by Wilcoxon matched-pairs signed rank test. (B) Baseline PSA levels in patients with omCRPC stratified by PSMA$^+$ and STEAP1$^+$ EV levels (n = 79). Bars represent medians and 95% confidence intervals. **$P < .01$ by Mann-Whitney $U$ test. (C) Baseline levels of PSMA- and STEAP1-positive EVs in patients stratified by the number of metastatic lesions identified by $^{11}$C-choline PET imaging; 1 lesion (n = 53), 2 lesions (n = 20), or 3 lesions (n = 6). ns = not significant, by Kruskal-Wallis test.

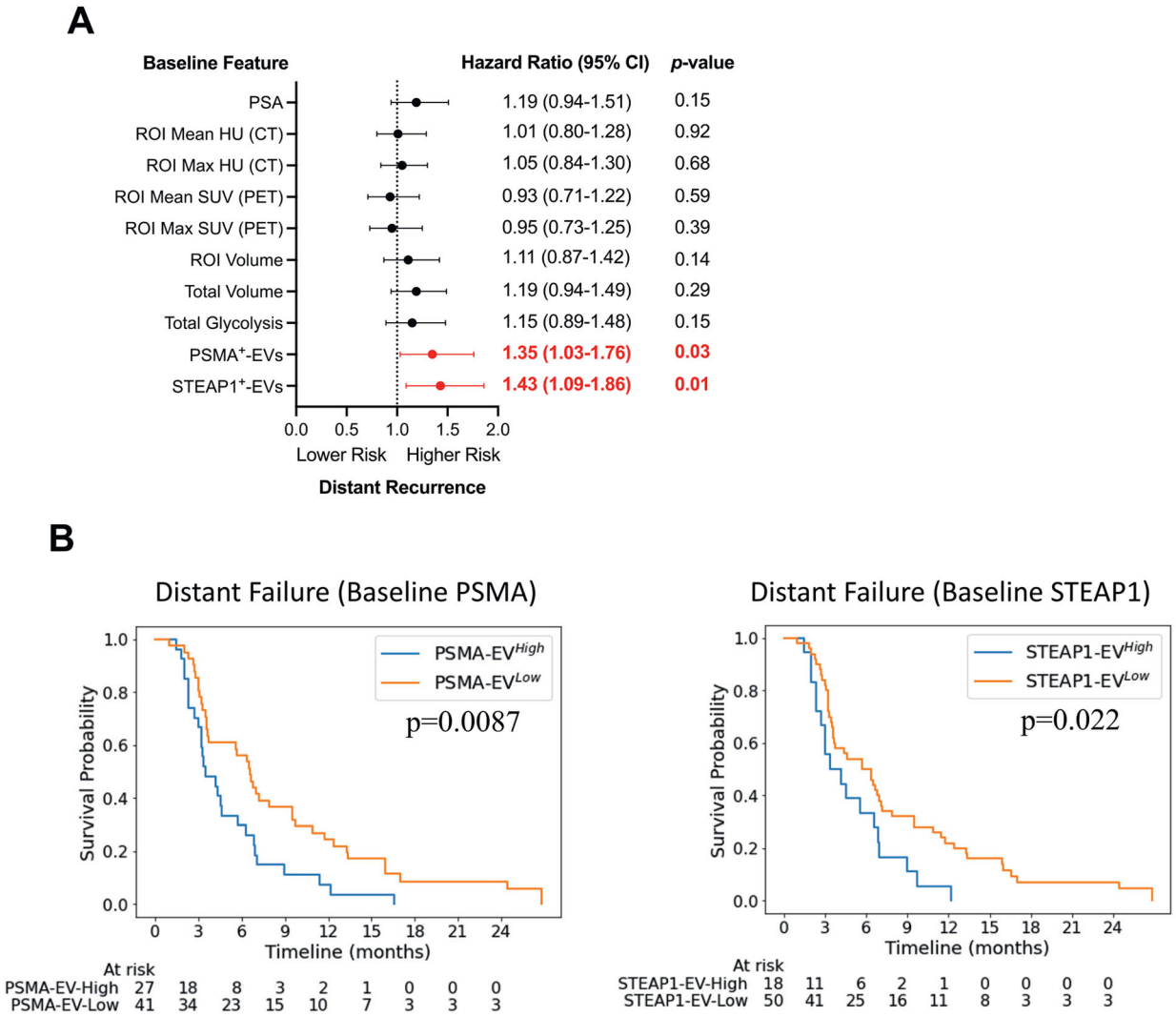


**Fig. 3.**

Baseline prostate cancerfispecific extracellular vesicles (PCEVs) predict risk of distant failure in oligometastatic castration-resistant prostate cancer (omCRPC) treated with SABR. (A) Forest plot of univariate Cox regression analysis between clinical factors, PCEV levels, and risk of distant failure. For $PSMA^+$ EVs: hazard ratio (HR), 1.35; 95% confidence interval (CI), 1.03–1.76; $P = .03$; n = 68. For $STEAP1^+$ EVs: HR, 1.43; 95% CI, 1.09–1.86; $P = .01$; n = 68. (B) Kaplan-Meier estimates of distant failure comparing patients with omCRPC who had high and low baseline levels of $PSMA^+$ EVs (B) and $STEAP1^+$ EVs (C) and treated with SABR. The median times to distant failure for high levels and low levels of $PSMA^+$ EVs were 3.47 months and 6.6 months, respectively ($P = .0087$). The median times to distant failure for high levels and low levels of $STEAP1^+$ EVs were 4.2 months and 5.73 months, respectively ($P = .022$).

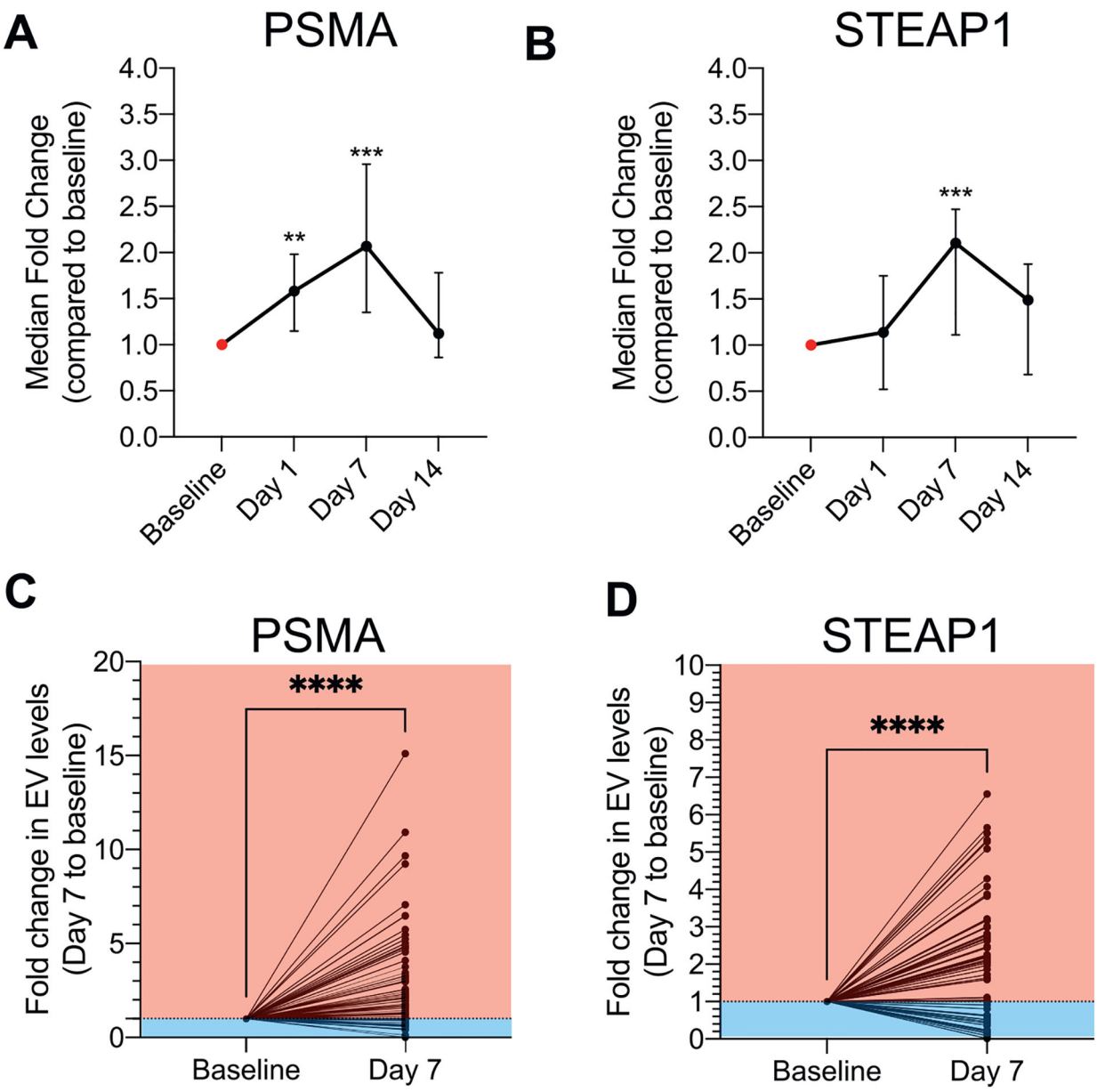


**Fig. 4.**

Kinetics of blood levels of prostate cancer–specific extracellular vesicles in patients with oligometastatic castration-resistant prostate cancer treated with SABR. (A, B) Changes in $PSMA^+$ extracellular vesicles (EVs) (A) and $STEAP1^+$ EVs (B) at 1, 7, and 14 days after SABR (n = 53). Data are presented as the median fold changes compared with baseline and 95% confidence intervals. $^{**}P < .01$ and $^{***}P < .001$ by Kruskal-Wallis test. (C, D) Fold change in levels of $PSMA^+$ EVs (C) and $STEAP1^+$ EVs (D) between baseline (pre-SABR) and day 7 after SABR. $^{****}P < .0001$ by Mann-Whitney *U* test (n = 66).

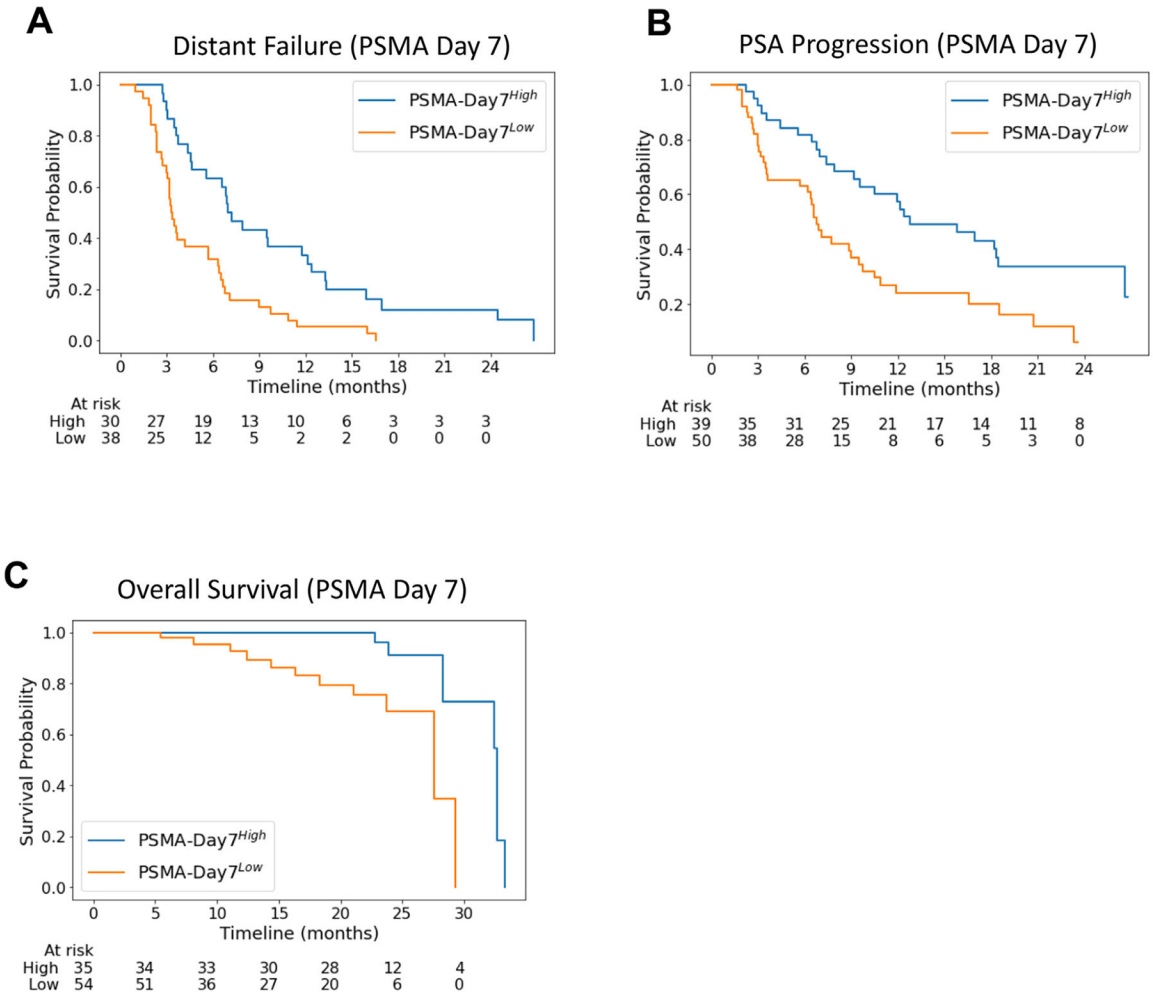


**Fig. 5.**

PSMA$^+$ extracellular vesicle (EV) levels SABR are predictors of oncological outcomes. Kaplan-Meier estimates of distant failure (A), prostate-specific antigen progression (B), and overall survival (C), comparing patients who had high and low baseline levels of PSMA$^+$ EVs. (D) Fold change in blood levels of PSMA$^+$ EVs at day 7 after SABR in patients presenting distant recurrence within 6 months (left) and no distant recurrence within 12 months (right).

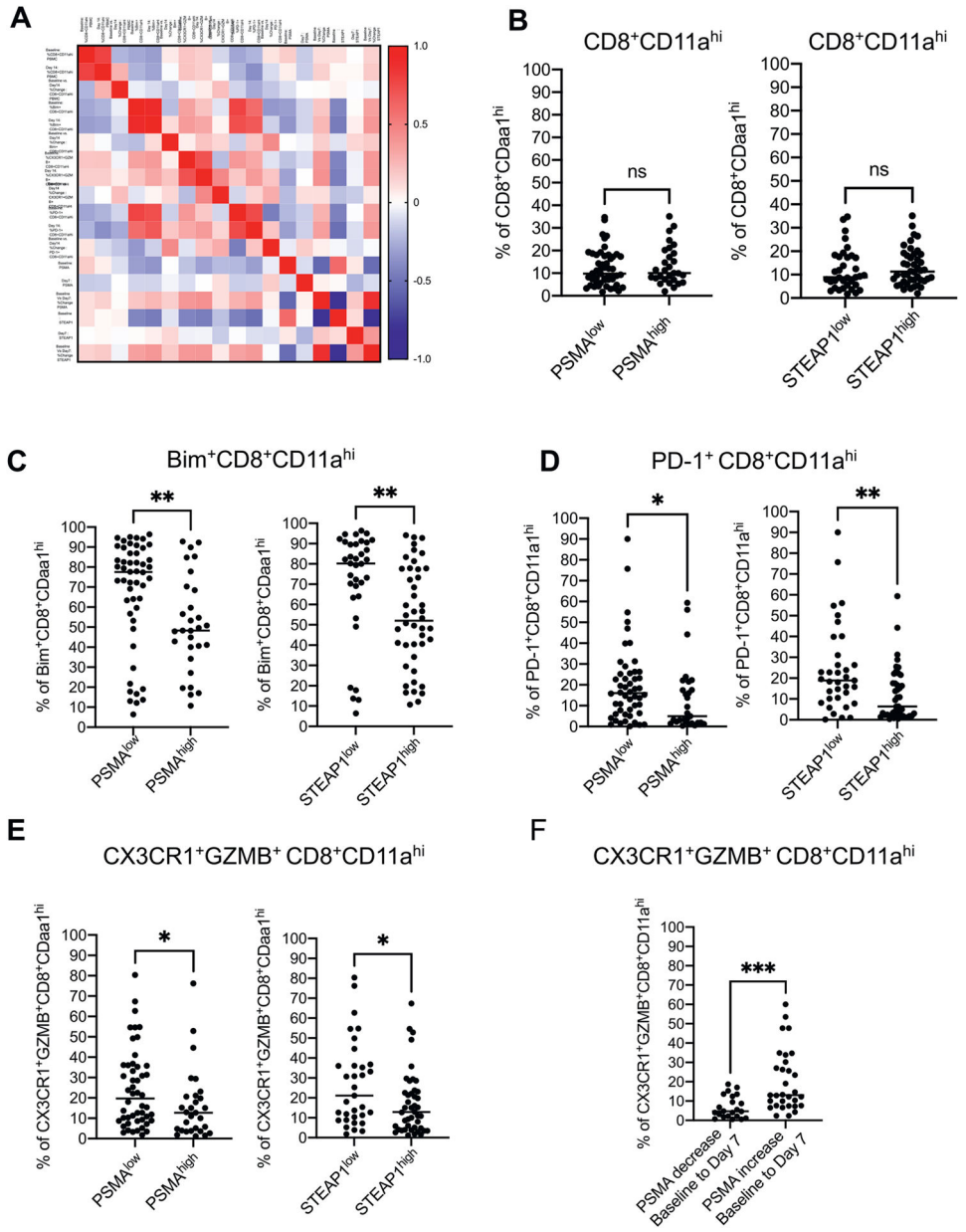


**Fig. 6.**

Association of prostate cancer–specific extracellular vesicle (PCEV) concentrations at baseline and after SABR with levels of tumor-reactive effector CD8 T cells. (A) Correlation matrix of PCEV levels and various subpopulations of peripheral CD8 T cells at baseline and after SABR. Spearman correlation coefficients are shown from −1.0 (blue) to 1.0 (red). (C-E) Baseline levels of subpopulations of tumor-reactive CD8 T cells in patients stratified by baseline concentrations of PCEVs. Levels of parent tumor-reactive CD8 T cells (B) and populations positive for $Bim^+$ (C), $PD\text{-}1^+$ (D), and $CX3CR1^+$ $GRZB^+$ (E) were compared in patients with low and high PCEV. (F) Levels of $CX3CR1^+$ $GRZB^+$ tumor-reactive CD8 T cells at day 14 in patients with increased or decreased $PSMA^+$ EV concentrations at day

7 (compared with baseline). *$P < .05$, **$P < .01$, ***$P < .001$, and ns = not significant, by Mann-Whitney $U$ test.